Journal of Solid State Chemistry **163,** 178–185 (2002)
doi:10.1006/jssc.2001.9390, available online at http://www.idealibrary.com on IDEAL®

On the System Silicon–Ytterbium:

Constitution, Crystal Chemistry, and Physical Properties

A. Grytsiv,* D. Kaczorowski,† A. Leithe-Jasper,* V. H. Tran,† A. Pikul,† P. Rogl,[1,]* M. Potel,‡ H. Noël,] M. Bohn,§ and T. Velikanova⊥

*Institut für Physikalische Chemie, Universität Wien, Währingerstraße 42, A-1090 Wien, Austria; †W. Trzebiatowski Institute for Low Temperature and Structure Research, Polish Academy of Sciences, P.O. Box 1410, P-50-950 Wroclaw, Poland; ‡Laboratoire de Chimie du Solide et Inorganique Moléculaire, UMR CNRS 6511, Université de Rennes I, Avenue du Général Leclerc, F-35042 Rennes Cedex, France; §CNRS-URA 1278, Centre de la Microsonde Electronique de l'Ouest, IFREMER, F-29263 Plouzanë, Brest, France; and ⊥Institute for Problems of Materials Science, Krzhyzhanovsky 3, Kiev, Ukraine

Received April 25, 2001; in revised form August 21, 2001; accepted September 7, 2001

Phase equilibria in the silicon-rich part of the system Si–Yb (> 60 at.% Si) have been established from DTA, LOM, EMPA, and X-ray diffraction experiments on arc-melted and annealed bulk alloys as well as on single crystals grown from pure gallium or indium metal used as a flux solvent. Phase relations are characterized by the existence of a defect disilicide showing polymorphism. Yb_3Si_5, the low-temperature modification with Th_3Pd_5 type, is a line compound at 62.5 at.% Si, stable below $947 \pm 7^\circ$C. Above this temperature Yb_3Si_5 transforms into the $YbSi_{2-x}$ (defect AlB_2-derivative type) corresponding to a peritectoid equilibrium at $947 \pm 7^\circ$C: $YbSi_{2-x} + YbSi \Leftrightarrow Yb_3Si_5$. $YbSi_{2-x}$ exhibits a small homogeneity region from ~ 62.5 at.% to ~ 63.5 at.% Si and melts incongruently at $1408 \pm 9^\circ$C at ~ 63 at.% Si. On cooling it decomposes according to a eutectoid reaction at $763 \pm 7^\circ$C: $YbSi_{2-x} \Leftrightarrow Yb_3Si_5 + (Si)$. The silicon-rich part of the diagram is characterized by a eutectic equilibrium at $1135 + 7^\circ$C and ~ 81 at.% Si: $L \Leftrightarrow YbSi_{2-x} + (Si)$. From magnetic susceptibility and electrical resistivity measurements, performed on single-crystalline specimens, Yb_3Si_5 was found to be an intermediate valent system. © 2002 Elsevier Science

Key Words: **phase diagram of Si–Yb (> 60 at.% Si); high-temperature modification of $YbSi_{2-x}$ with AlB_2-derivative type; low-temperature modification of Yb_3Si_5 with Th_3Pd_5 type; intermediate valent system.**

INTRODUCTION

Transition metal disilicides have gained some interest not only as electric contact materials in Si-wafer-based electronic devices, but even more so in optical fiber telecommunications because of sharply structured photoluminescence bands from rare earth intra-4*f*-shell transitions (1). Rare earth silicide films were found to form the lowest Schottky barriers on *n*-type silicon and Schottky contacts on *p*-type silicon, attractive features in the design of infrared detectors (2, 3). Formation of silicides via a rare earth thin-film to substrate reaction may proceed from as low as 300°C (4); the kinetics and interface formation, however, are still poorly understood. Although many binary rare earth–silicon systems have been critically assessed (5) to provide the necessary phase diagram information, there is still a serious lack of information on the phase equilibria of the Si–Yb system (5). Part of this problem is certainly due to the rather low melting and boiling point of ytterbium metal ($T_m = 819^\circ$C, $T_b = 1194^\circ$C (5)), which makes controlled synthesis of single-phase ytterbium compounds generally difficult to accomplish via the usual high-frequency or arc-melting techniques. So far only four binary Si–Yb phases have been identified from cursory crystallographic inspections indicating complicated defect ordering of atom sublattices (see (5) and references therein). A recent single-crystal study of Yb_3Si_5 (6) confirmed the Th_3Pd_5 type earlier assigned by Iandelli *et al.* (7). Table 1 comprises a listing of all crystallographic data available in literature on the phases pertinent to the Si–Yb binary. From magnetic susceptibility measurements in the limited range, $90 < T < 1000$ K, the two compounds richest in Si, $YbSi_{1.8}$ and Yb_3Si_5, were reported to be temperature-induced valence fluctuators (7). A photoemission study (8) confirmed a room-temperature valence of $Yb^{2.6+}$ in Yb_3Si_5. No details were given for the low-temperature region.

Based on the lack of comprehensive data, the present paper thus intends to provide the hitherto missing information on phase equilibria, crystallographic information, and the physical behavior of the compounds in the silicon-rich part of the Si–Yb constitution diagram. The detailed inspection of the constitution, crystal chemistry, and physical

[1] To whom correspondence should be addressed. E-mail: peter.franz.rogl@univie.ac.at.

0022-4596/02 $35.00

TABLE 1
Crystallographic Data for the Binary Compounds in the Si–Yb System (Literature)

Phase	Pearson symbol	Space group	Structure type	Lattice parameters in nm			Reference
				a	*b*	*c*	
Yb_5Si_3	hP16	$P6_3/mcm$	Mn_5Si_3	0.8215	—	0.6186	(5, 24)
YbSi	oC8	*Cmcm*	CrB	0.4178	1.031	0.3768	(5, 24)
Yb_3Si_5	hP8	$P\bar{6}2m$	Th_3Pd_5	0.6508	—	0.4092	(6)
				0.6512	—	0.4090	(7, 24)
$YbSi_{2-x}$	hP3	*P6/mmm*	AlB_2	0.3771	—	0.4098	(24)
				0.3784	—	0.4098	(7, 24), $0.3 < x < 0.14$

properties of the compounds in the silicon-rich part of the system was achieved with single crystals. In a recent paper (9) we demonstrated the use of the Lebeau method (9, 10) for the growth of sizable single-crystal material, a technique successfully used in the past to produce transition metal borides as well as silicides from tin, copper, or aluminum flux (11, 12). When the use of Zn flux in the early stages of the project, however, prompted the formation of novel ternary silicides, $YbZn_2Si_2$ and $Yb(Zn,Si)_{2-x}$ (9), we attempted to explore rather inert flux systems such as Ga or In.

EXPERIMENTAL

Bulk alloys, each with a total weight of 5 to 10 g, were synthesized by repeated argon arc-melting ingots of the elements of 99.9 mass% minimum purity on a water-cooled copper hearth and a tungsten electrode under Ti-gettered high-purity argon. All weight losses were attributed to evaporation of ytterbium. In most cases a 13Yb87Si master alloy was used instead of pure Si in order to significantly reduce evaporation losses.

Differential thermal analysis was performed on as-cast alloys at a heating rate of $50^\circ C\,min^{-1}$ under helium employing Sc_2O_3 crucibles and a W/WRe20 thermocouple calibrated against the international temperature scale IPTS-91.

X-ray investigation was performed after homogenization of parts of the alloy buttons, which were vacuum-sealed in quartz capillaries and annealed at 700°C or 600°C, respectively, for up to 140 h prior to quenching in cold water.

Light optical microscopy (LOM) on selected alloys, which have been polished and etched by standard methods, and electron microprobe analyses (EMPA) based on wavelength-dispersive X-ray spectroscopy were used to examine phase equilibria and equilibrium compositions. For quantitative EMPA in a CAMEBAX system the sample compositions were evaluated comparing the X-ray intensities of the elements (Yb$L\alpha$ and Si$K\alpha$) in the alloy with those of pure elemental standards after application of an iterative ZAF correction (acceleration voltage, 15 kV; counting time, 20 sec) (13). Single-line EMPA scans across the annealed alloys assured constant element profiles and thereby indicated alloy homogeneity and equilibrium condition.

Single-crystal material was obtained via the Lebeau method (10) essentially based on the temperature-dependent solubility of Yb and Si in the metal flux (Ga,In), which was contained in Al_2O_3 crucibles vacuum-sealed within thick-walled quartz tubes. The materials used were 5 N gallium ingots from Alcan Electronics, CH, indium ingots, 99.9% pure, from Ögussa, A, 99.9% pure ingots of ytterbium from Auer Remy, D, which were reduced to filings under cyclohexane, and Si pieces, 99.99 mass%, from Alfa Ventron, D. A typical experiment started from room temperature with a heating rate of $75^\circ C\,h^{-1}$ up to 1050 to 1100°C with an intermediate hold at 200°C for 1 h slightly above the melting point of the flux. After a soaking period at the top temperature for up to 12 h, cooling to 600°C proceeded at a speed of $25^\circ C\,h^{-1}$, after which the sample batches were kept at 600°C for 12 h prior to final quenching, when samples were simply removed from the hot furnace. Starting from various ratios (Yb + Si)/flux, the heating and cooling rates were sufficient to produce good-quality single-crystal specimens of the ytterbium silicides. Gallium- or indium-containing flux was usually removed in an ultrasonic bath of mercury at room temperature.

Crystal identification was performed for a series of crystal specimens using a 57.3-mm radius Gandolfi camera, which also served for determination of the unit cell dimensions. In some cases, precise lattice parameters and standard deviations were obtained by a least-squares refinement of room temperature Guinier-Huber X-ray (Cu$K\alpha_1$) powder data from a set of crystals (optically selected under the microscope and powdered) employing an internal standard of 99.9999 mass% pure Ge ($a_{Ge} = 0.5657906$ nm). Weissenberg photographs accomplished crystal quality control and inspection of crystal symmetry. Single-crystal X-ray intensity data for Yb_3Si_5 were collected for a hemisphere of 211 images in a total exposure time of 71 min on a four-circle

Nonius Kappa diffractometer equipped with a CCD area detector employing graphite-monochromated Mo$K\alpha$ radiation ($\lambda = 0.071073$ nm). Orientation matrix and unit cell parameters were derived from the first 10 data frames using the program DENZO (14). Absorption correction was taken from the program SORTAV (14) ($\mu = 47.1\ \mathrm{mm}^{-1}$). The structure was refined with the aid of the SHELXS-97 program (15).

For some alloys quantitative refinement of the atom positions was based on the X-ray intensity data obtained from a flat specimen in a Siemens D5000 automatic powder diffractometer (Cu$K\alpha$) or in a Guinier-Huber image plate recording system (Cu$K\alpha_1$). Full-matrix–full-profile Rietveld refinements have been performed employing the FULLPROF program (16).

Magnetic measurements were performed in the temperature range 1.7–800 K in magnetic fields up to 5 T using a Quantum Design MPMS-5 SQUID magnetometer. For these studies a collection of single crystals freely placed in a sample holder was used.

Electrical resistivity was measured in the range 4.2–300 K employing a conventional dc four-point technique. In these measurements the specimens were needle-shaped single crystals with the electrical leads attached by silver epoxy paste.

RESULTS AND DISCUSSION

a. Crystal Structure of Yb_3Si_5 with the Th_3Pd_5 Type

In order to probe the potential of a suitable flux for the synthesis of Yb silicides, several batches with different flux systems (pure Zn, Ga, or pure In) were subject to elaborate temperature programs. It is interesting to note that pure Zn or Ga flux was less efficient to produce high-quality and sizable single-crystal material, whereas In flux reproducibly resulted in good quality and large single crystals of Yb_3Si_5. Dissolution of the flux led to residues of in most cases rather well shaped crystals (> 0.25 mm). With respect to the strong tendency observed in defect rare earth disilicides for vacancy ordering in terms of various superstructure types (17, 18), a detailed inspection of vacancy ordering was performed in our X-ray data. However, Weissenberg photographs taken along [00.1] as well as the CCD reciprocal lattice representations for rotation axes [00.1] and [10.0] gave no indication of superstructures or deviation from a primitive hexagonal cell with $a \sim 0.65$ and $c \sim 0.41$ nm. The absence of systematic extinctions is compatible with the space group $P\bar{6}2m$ (D_{3h}^3, No. 189) assigned in earlier investigations (6, 7). Starting from the atomic arrangements in the Th_3Pd_5 type presented earlier (6, 7), structure refinement for Yb_3Si_5 converged without difficulties to residual values as low as 0.026. Results of the structural refinements are given in Table 2 including various residual values, anisotropic thermal parameters, and interatomic distances. A listing of the intensity data may be obtained from the authors on request. There is fine agreement within the results obtained with the literature data presented, proving the fully ordered character of the defects in the AlB_2-type parent Si layers consistent with the description in the Th_3Pd_5 type. The crystallographic group–subgroup relationship among the structure types AlB_2 ($Yb_3Si_5\square$) to Th_3Pd_5 was already discussed (6, 7) in combination with the results from a semi-empirical band structure calculation on the basis of an extended Hückel formalism (6).

TABLE 2
Structure Refinement[a] for X-Ray Single-Crystal Data of Yb_3Si_5

Parameter/compound			
Lattice parameters (nm)	$a = 0.65152(2)$; $c = 0.40911(2)$		
Space group, Z	$P\bar{6}2m$, origin at $\bar{6}2m$, $Z = 1$		
Structure type	Th_3Pd_5		
Density, ρ_{X-ray} (Mg m^{-3})	7.28		
Data collection; X-rays	Nonius Kappa CCD; Mo$K\alpha_1$		
2Θ range (deg)	2.0 to 80.5		
Number of variables	12		
Reflections in refinement	215 ($214 > 2\sigma$) (meas. 3362)		
$R_I = \sum\|I_o - I_c\|/\sum I_o$	0.026 ($I > 2\sigma$); R_I (all data) = 0.064		
$R_w = [\sum w_i\|y_{oi} - y_{ci}\|^2/\sum w_i\|y_{oi}\|^2]^{1/2}$	0.066		
Overall R_{merge}	0.065		
Goodness of fit	1.12		
Atom parameters			
	Yb in $3g$ ($x = 0.64215(9)$, 0, $\frac{1}{2}$)		
$U_{eq.}(U_{iso})$ 10^2 (nm^2)	0.0058(2)[b]		
	Si1 in $3f$ ($x = 0.2673(8)$, 0, 0)		
$U_{eq.}(U_{iso})$ 10^2 (nm^2)	0.0088(7)[b]		
	Si2 in $2c$ ($\frac{1}{3}$, $\frac{2}{3}$, 0)		
$U_{eq.}(U_{iso})$ 10^2 (nm^2)	0.0073(9)[b]		
Distances (nm) < 0.40000 nm;	Yb	2Si2	0.29298
standard deviations < 0.00006 nm		2Si2	0.29300
		4Si1	0.29301
		2Si1	0.31875
CN = 14		4Yb	0.36329
	Si1	1Si2	0.24154
		1Si2	0.24160
		4Yb	0.29301
		2Si1	0.30164
CN = 10		2Yb	0.31875
	Si2	1Si1	0.24154
		1Si1	0.24158
		1Si1	0.24160
		2Yb	0.29298
CN = 9		2Yb	0.29300

[a] Crystal structure data were standardized using Program Typix (23).

[b] Anisotropic displacement factors (10^2 nm^2). Yb: $U_{11} = 0.0064(2)$, $U_{22} = 0.0043(2)$, $U_{33} = 0.0060(3)$, $U_{12} = U_{13}$, $U_{23} = 0.0021(1)$. Si1: $U_{11} = 0.0113(1)$, $U_{22} = 0.005(1)$, $U_{33} = 0.006(1)$, $U_{12} = U_{13}$, $U_{23} = 0.0026(7)$.

Si2: $U_{11} = 0.008(1)$, $U_{22} = 0.008(1)$, $U_{33} = 0.007(1)$, $U_{12} = U_{13}$, $U_{23} = 0.0038(6)$.

TABLE 3
Invariant Equilibria in the Si–Yb System (60–100 at.% Si)

Reaction	Composition of the respective phases (*EMPA*) in at.% Si			Temperature, °C
$L + YbSi \Leftrightarrow YbSi_{2-x}$	~ 67	50	~ 63	1408 ± 9
$L \Leftrightarrow (Si) + YbSi_{2-x}$	80.6	99.8	63.5	1135 ± 7
$YbSi_{2-x} + YbSi \Leftrightarrow Yb_3Si_5$	~ 62.5	50	62.5	947 ± 7
$YbSi_{2-x} \Leftrightarrow (Si) + Yb_3Si_5$	~ 63	99.9	62.5	763 ± 5

The X-ray pattern of the Th_3Pd_5 type is well resolved also from powder Rietveld refinement of single-phase Yb_3Si_5 samples prepared by arc-melting and subsequent annealing at 700°C. Furthermore the Th_3Pd_5 structure was also well refined in the case of two-phase samples containing YbSi; however, X-ray profiles of samples containing free silicon were not consistent with the simple models of AlB_2 or/and Th_3Pd_5 types. In silicon-rich as-cast samples we observed a number of weak reflections, which belong to neither the AlB_2 nor the Th_3Pd_5 structure. The angular position of these reflections slightly varies from sample to sample, but these reflections are never observed in samples annealed at 600 or 700°C. On the other hand, in annealed samples we find reflections at the Bragg positions characteristic of the Th_3Pd_5 structure, which on close examination reveal a double-peak feature. As a consequence, the crystal chemistry of ytterbium disilicide is certainly more complicated than reported (7): at high temperatures $YbSi_{2-x}$ exists as AlB_2-derivative type structure(s) (labeled as AlB_2-der.), while at low temperature Yb_3Si_5 adopts simple Th_3Pd_5 type in equilibrium with YbSi but Th_3Pd_5-derivative type structure(s) in equilibrium with Si (labeled as Th_3Pd_5–der.).

b. The Constitution Diagram of Si–Yb for > 60 at.% Si

Table 3 and Fig. 1 present the isothermal reactions and the phase equilibria in the Si–Yb diagram (60–100 at.% Si) constructed on the basis of the X-ray, micrographic, EMPA, and DTA investigations.

The metallographic analysis of the as-cast alloys clearly shows the eutectic involving silicon and $YbSi_{2-x}$ (Fig. 2). The location of the eutectic was established by electron microprobe large area scans (80–81 at.% Si) and DTA measurements (1135 ± 7°C) of as-cast alloys containing free silicon. As we can see from Table 4, lattice parameters of $YbSi_{2-x}$ in the as-cast state vary from sample to sample and this fact indicates a small homogeneity region for this phase.

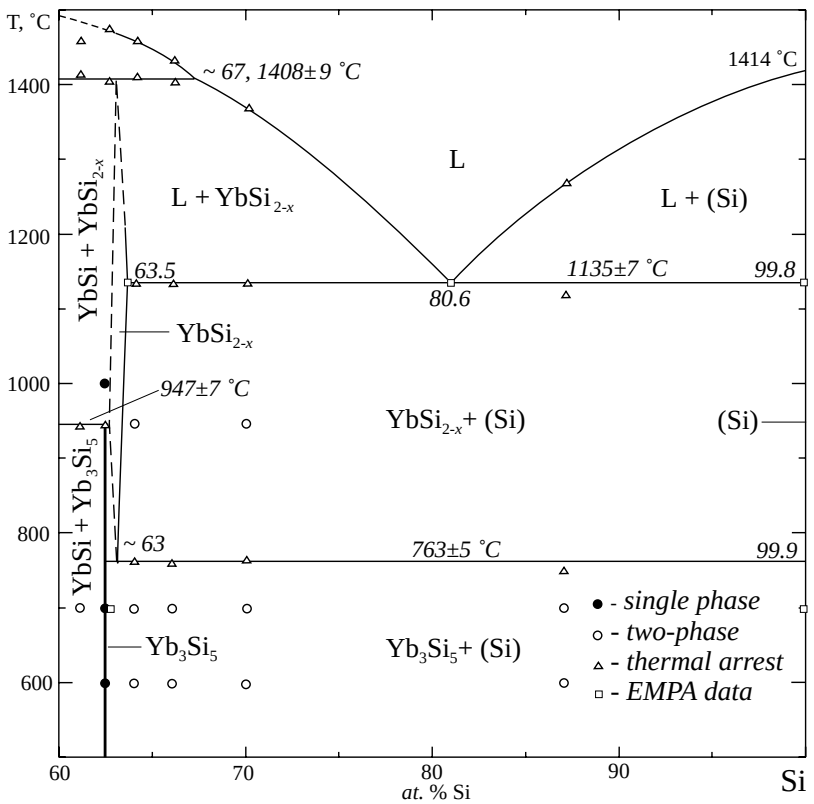

FIG. 1. Partial phase diagram Si–Yb for 60 to 100 at.% Si.

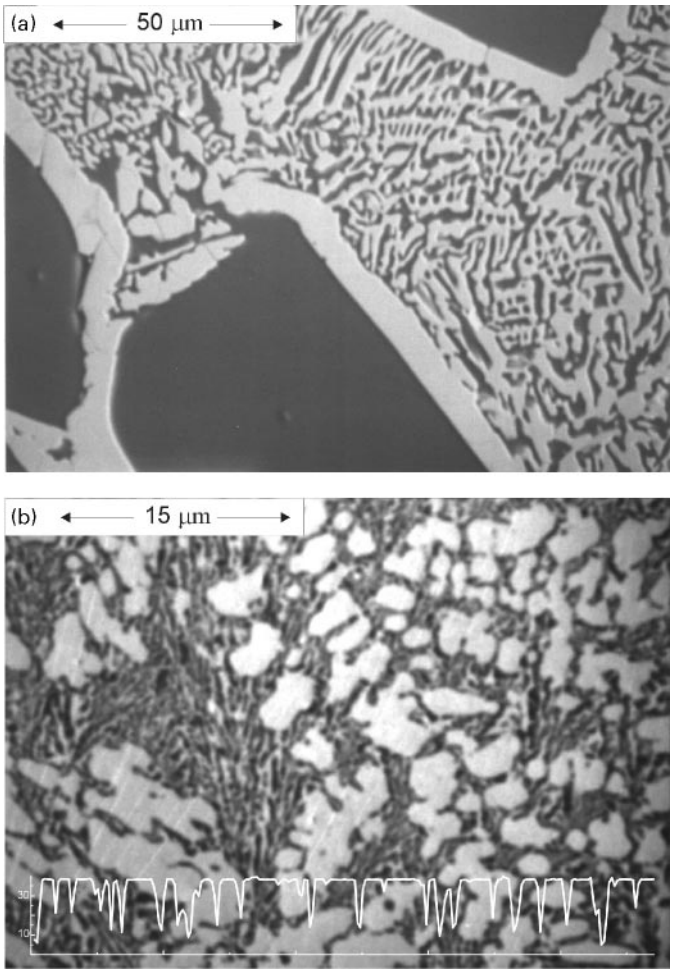

FIG. 2. Micrograph of as-cast samples: (a) 13Yb87Si (in at.%). Dark large crystals are Si enclosed by bright seams of $YbSi_{2-x}$ in eutectic matrix (Si) + $YbSi_{2-x}$. (b) 30Yb70Si (in at.%). Light crystals of $YbSi_{2-x}$ in eutectic matrix (Si) + $YbSi_{2-x}$. Inset: EMPA scan of Yb content (in at.%) across grains of $YbSi_{2-x}$. The flat plateaus and the sharp edges in concentration confirm the absence of concentration gradients, i.e., the absence of homogeneity regions.

From the experimental data obtained we conclude that $YbSi_{2-x}$ and Yb_3Si_5 are polymorphs of the temperature–concentration type; both silicides coexist in equilibrium with silicon. This fact contradicts the result of Iandelli *et al.* (5, 7), who reported that only $YbSi_{2-x}$ with the AlB_2 type coexists in equilibrium with silicon. The temperatures of solid phase transformations involving $YbSi_{2-x}$ and Yb_3Si_5 were established by DTA (Table 4), revealing 763 ± 5°C for the silicon-containing samples, and 947 ± 7°C for single-phase Yb_3Si_5 and samples richer in ytterbium. The temperature of 763 ± 5°C corresponds to the eutectoid invariant equilibrium $YbSi_{2-x} \Leftrightarrow Yb_3Si_5$ + (Si). The type of the transformation at 947 ± 7°C is difficult to establish due to close temperature values of the solid phase transformation for single phase Yb_3Si_5 and two-phase Yb_3Si_5 + YbSi alloys. Yb_3Si_5 shows disordered crystal structure on the silicon-rich side and has a rather narrow homogeneity region. It can be seen from DTA and EMPA data as well as from a comparison of unit cell dimensions of Si-rich and Si-poor Yb_3Si_5 (Table 4). For the single-phase sample of Yb_3Si_5 the temperature of the solid phase transformation (735°C) on cooling (invariant reaction $YbSi + YbSi_{2-x} \Leftrightarrow Yb_3Si_5$) is much lower than that on heating (947°C). It seems that during DTA measurements in an open crucible under He gas the composition of this alloy was changed due to ytterbium evaporation for less than 0.7 at.% into the silicon-rich part and correspondingly the temperature of another solid phase transformation $YbSi_{2-x} \Leftrightarrow Yb_3Si_5$ + (Si) was measured on cooling.

The thermal arrests at 1408 ± 9°C were determined for alloys containing less than 70 at.% Si. This temperature was attributed to a peritectic equilibrium $L + YbSi \Leftrightarrow YbSi_{2-x}$. The composition of the liquid taking part in this equilibrium lies between 64 and 70 at.% Si (67 at.% Si is the accepted value). The maximal silicon content in $YbSi_{2-x}$ (63.5 at.% Si) was established by EMPA and agrees with the facts that we can see a small amount of eutectic on micrographs of the as-cast alloy $Yb_{36}Si_{64}$ and the DTA curve shows a very weak thermal arrest at 1130°C corresponding to this eutectic. The value of 63.5 at.% Si is close to the formula $YbSi_{1.8}$ reported in (7) for the silicon-rich ytterbium silicide with AlB_2 type.

With respect to the phase equilibria established in Fig. 2a, the observation of nanosized YbSi precipitates after Yb ion implementation into Si(001) wafers and 10 min anneal at temperatures as high as 1200°C (1) can only be conceived as metastable phase formation, keeping in mind that for instance at 1200°C the only equilibrium phases are (Si) + liquid and below the eutectic at 1135°C are (Si) + $YbSi_{2-x}$.

c. Physical Properties of Yb_3Si_5

c.1. Magnetism. Figure 3 displays the magnetic susceptibility of single-crystalline Yb_3Si_5, measured up to 800 K in a field of 0.5 T. The magnetic susceptibility is small and weakly temperature dependent (except at low temperatures). The temperature variation of the susceptibility shows a broad shallow maximum around T [χ(max)] = 100 K. Apparently no Curie–Weiss behavior is observed at ambient temperatures.

The overall shape of $\chi(T)$ of Yb_3Si_5 is reminiscent of an intermediate valence system. As there is only one crystallographic position for metal atoms, one could expect the occurrence of a noninteger valence of the ytterbium atoms, which changes with temperature. Accordingly, the experimental $\chi(T)$ data can be checked with respect to the interconfiguration fluctuation model (ICF) of Sales and Wohlleben (19). In the scope of that approach the magnetic susceptibility of an ytterbium-based compound with a non

TABLE 4
Crystallographic, EMPA, and DTA Data for Selected Samples in the Binary Si–Yb System

Nominal[a] Compos. in at.%Si	Heat treatment	Phase analysis	Space group	Structure type	Lattice parameters in nm			EMPA in at.%Si	Thermal arests in DTA		
					a	*b*	*c*		$T_{heating}$, °C	$T_{cooling}$, °C	Invariant reaction or phase boundary
61	As-cast	Yb_3Si_5	$P\bar{6}2m$	Th_3Pd_5	0.6511(1)		0.4089(1)		945	915	$YbSi_{2-x} + YbSi = Yb_3Si_5$
		YbSi	*Cmcm*	CrB	0.4179(2)	1.0309(7)	0.37606(9)		1415	—	$L + YbSi = YbSi_{2-x}$
	400 h/ 700°C	Yb_3Si_5	$P\bar{6}2m$	Th_3Pd_5	0.65150(1)		0.40915(1)		1460	1440	L/L + YbSi
		YbSi	*Cmcm*	CrB	0.41803(3)	1.0313(1)	0.37622(2)				
62.5	As-cast	Yb_3Si_5		Th_3Pd_5	0.65116(2)		0.40911(6)		947	735[d]	$YbSi_{2-x} + YbSi = Yb_3Si_5$
	400 h/ 700°C	Yb_3Si_5	$P\bar{6}2m$	Th_3Pd_5	0.65112(3)		0.40907(6)		1403	1330	$L + YbSi = YbSi_{2-x}$
									1470	1430	L/L + YbSi
64.0	As-cast	$YbSi_{2-x}$		AlB_2-der.[b]	0.37823(6)		0.40985(7)	63.1	765	700	$YbSi_{2-x} = (Si) + Yb_3Si_5$
		(Si)	$Fd\bar{3}m$	$C_{diamond}$	Traces			99.8	1135	1130	$L_e = (Si) + YbSi_{2-x}$
								Eu:[e] 80.8	1410	1385	$L + YbSi = YbSi_{2-x}$
	140 h/ 700°C	Yb_3Si_5		Th_3Pd_5-der.[c]	0.65140(8)		0.40913(7)	62.8	1425	1460	Nonindexed
		(Si)	$Fd\bar{3}m$	$C_{diamond}$	Traces			99.9	1460	1430	L/L + YbSi
66.0	As-cast	$YbSi_{2-x}$		AlB_2-der.	0.37803(7)		0.4096(1)	63.5	760	715	$YbSi_{2-x} = (Si) + Yb_3Si_5$
		(Si)	$Fd\bar{3}m$	$C_{diamond}$	Traces			99.8	1135	1130	$L_e = (Si) + YbSi_{2-x}$
								Eu: 79.8	1400	1375	$L + YbSi = YbSi_{2-x}$
	140 h/ 700°C	Yb_3Si_5		Th_3Pd_5-der.	0.65139(7)		0.4091(1)	62.9	1435	1400	L/L + YbSi
		(Si)	$Fd\bar{3}m$	$C_{diamond}$	0.5431(3)			99.9			
70.0	As-cast	$YbSi_{2-x}$		AlB_2-der.	0.37786(2)		0.40978(5)	63.2	765	715	$YbSi_{2-x} = (Si) + Yb_3Si_5$
		(Si)	$Fd\bar{3}m$	$C_{diamond}$	Traces			99.8	1135	1140	$L_e = (Si) + YbSi_{2-x}$
								Eu: 81.1	1370	1385	$L/L + YbSi_{2-x}$
87.0	As-cast	$YbSi_{2-x}$		AlB_2-der.	0.37707(9)		0.4095(1)	63.3	750	720	$YbSi_{2-x} = (Si) + Yb_3Si_5$
		(Si)	$Fd\bar{3}m$	$C_{diamond}$	0.54297(4)			99.9	1120	1128	$L_e = (Si) + YbSi_{2-x}$
								Eu: 80.6	1270	1240	L/L + (Si)

[a] Nominal composition corrected for Yb losses during melting.
[b] Structure derived from AlB_2 type, subcell only.
[c] Structure derived from Th_3Pd_5 type, subcell only.
[d] Arrest corresponds to the invariant reaction: $YbSi_{2-x} \Leftrightarrow (Si) + Yb_3Si_5$.
[e] Composition of eutectic.

magnetic $4f^{14}$ ground state configuration and a magnetic $4f^{13}$ excited state configuration is represented by

$$\chi_{sw}(T) = \frac{N\mu_{eff}^2[1 - v(T)]}{3k_B(T + T_{sf})},$$

where $\mu_{eff} = 4.54\ \mu_B$, T_{sf} is a spin fluctuation temperature, and $v(T)$ is a temperature-dependent mean occupation of the ground state given by

$$v(T) = \frac{1}{1 + 8\ \exp[-E_{ex}/k_B(T + T_{sf})]},$$

where E_{ex} is an energy gap between the ground and excited states.

In contrast to the ICF model which gives $\chi(T) = \text{const}$ for $T \to 0$, the experimental $\chi(T)$ curve presented in Fig. 3 shows a strong upturn at low temperatures. Although this behavior is different from that expected for intermediate

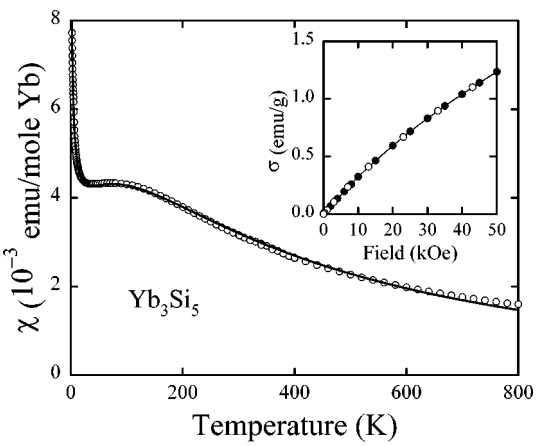

FIG. 3. Temperature dependence of the molar magnetic susceptibility of Yb_3Si_5. The solid lines are fits of the experimental data to the Sales–Wohlleben + Curie Weiss formula (see the text). Inset shows the field variation of the magnetization at 1.7 K with increasing (full circles) and decreasing (open circles) magnetic field.

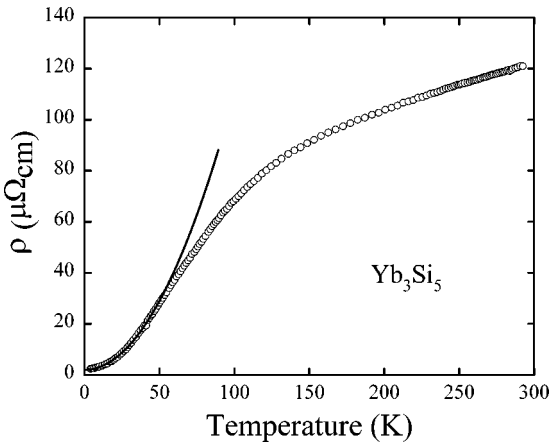

FIG. 4. Temperature variation of the electrical resistivity of Yb_3Si_5 along the *c*-axis. The solid lines mark a T^2 dependence of the resistivity.

valence systems, it is usually observed in real intermediate valent materials and attributed to magnetic impurities. In the present case these could be uncompensated Yb^{3+} ions on the crystal surface. Thus, in order to account for the presence of some small amount of uncompensated Yb^{+3} ions it was assumed that their contribution to the measured susceptibility is of a Curie–Weiss type. Moreover, other possible contributions due to conduction–electron paramagnetism, core-electron diamagnetism, and/or Van Vleck paramagnetism have also been considered by introducing a third term χ_0, independent of temperature. Thus, the experimental data were fitted to the following formula,

$$\chi(T) = \chi_{sw}(T) + \frac{C_{imp}}{T + \theta_{imp}} + \chi_0,$$

and the solid line in Fig. 4 represents the result of the fitting procedure. The agreement between the calculated and experimental data is satisfactory in the whole temperature range. For Yb_3Si_5 the fitting parameters are as follows: $T_{sf} = 177$ K, $E_{ex} = 561$ K, $C_{imp} = 0.023$ emu K/mole, $\theta_{imp} = 3$ K, and $\chi_0 = -7.2 \times 10^{-4}$ emu/mole. If one assumes that the impurity contribution stems from stable Yb^{3+} ions, their concentration ($n = C_{imp}/C_{Yb^{3+}}$ where $C_{Yb^{3+}} = \mu_{eff}^2/8$) is estimated as 0.9 at.% Yb^{3+} ions per mole of Yb_3Si_5. Such small amounts of impurities are obviously far below the detection limit of X-ray diffraction but fully account for the magnetic behavior observed at low temperatures. The effective valence of the ytterbium atom is 2.3 at helium temperature and already 2.8 at 800 K. Such a strong increase in the effective valence comes from thermal population of the excited state, located relatively close in energy. Accordingly, also the spin fluctuation temperature in Yb_3Si_5 is rather low. It is worth noting that the value of T_{sf} derived above within the ICF approach is consistent with the estimated T_{sf} (20),

$$T_{sf} = \tfrac{3}{2}\, T[\chi(\max)],$$

being about 150 K for Yb_3Si_5.

c.2. Electrical conductivity. Figure 4 shows the temperature dependence of the electrical resistivity of a single crystal of Yb_3Si_5, measured along the *c*-axis revealing metallic-like behavior with the room temperature resistivity of the order of 100 μΩ cm. The residual resistivity ratio $RRR = \rho(290\text{ K})/\rho(4.2\text{ K})$ is about 53. Above ca. 50 K the resistivity $\rho(T)$ shows a broad knee around 120 K and some tendency to saturation, reminiscent of spin fluctuations.

Below about 50 K the resistivity follows the equation

$$\rho(T) = \rho_0 + AT^2,$$

with the parameters $\rho_0 = 2$ μΩ cm and $A = 0.011$ μΩ cm/K^2. A T^2 variation of the low-temperature resistivity is characteristic of a Fermi liquid (20) and thus the electrical properties of Yb_3Si_5 seem to corroborate the intermediate valent character deduced from the magnetic data. Assuming that the universal relation $A/\gamma^2 = 10^{-5}$ μΩ cm (mole K/mJ)^2 (21), between the coefficient A and the linear coefficient of the electronic specific heat, is fulfilled, one can estimate γ as being about 30 mJ/mole/K^2 for Yb_3Si_5. It is worth recalling that such moderately enhanced values of γ are characteristic of intermediate valence systems (20, 22).

ACKNOWLEDGMENTS

This research was supported by the Austrian FWF under grant P9709 and the Austrian-Polish Scientific-Technical Exchange Program under project 13/99. Thanks are furthermore due to Dr. P. Martensyuk for the DTA measurements.

REFERENCES

1. Y. Yang, H. Chen, Y. Q. Zhou, and F. H. Li, *J. Mater. Sci.* **32,** 6665 (1997).
2. F. P. Netzer, *J. Phys.: Condens. Matter* **7,** 991 (1995).
3. T. V. Krachino, M. V. Kuz'min, M. V. Loginov, and M. A. Mittsev, *Physics of Low Dimensional Structures* **9–10,** 95 (1999).
4. G. Molnar, G. Peto, Z. E. Horvath, and E. Zsoldos, *Appl. Phys. Lett.* **64,** 1679 (1994).
5. "Binary Alloy Phase Diagrams" (T. B. Massalski, Ed.), 2nd ed. ASM, Materials Park, OH, 1990.
6. R. Pöttgen, R. D. Hoffmann, and D. Kussmann, *Z. Anorg. Allg. Chem.* **624,** 945 (1998).
7. A. Iandelli, P. Palenzona, and G. L. Olcese, *J. Less-Common Met.* **64,** 213 (1979).
8. I. Abbiati, L. Braicovich, U. Del Pennino, A. Iandelli, G. L. Olcese, A. Palenzona, C. Carbone, J. Nogami, J. J Yeh, and I. Lindau, *Physica* **130B,** 141 (1985).

9. A. Grytsiv, A. Leithe-Jasper, H. Flandorfer, P. Rogl, K. Hiebl, C. Godart, and T. Velikanova, *J. Alloys Compds* **266,** 7 (1998).
10. P. Lebeau and J. Figueras, *C. R. Acad. Sci., Paris* **136,** 1329 (1903).
11. D. Elwell and H. J. Scheel, "Crystal Growth from High-Temperature Solutions." Academic Press, London, 1975.
12. S. Okada, T. Atoda, I. Higashi, and Y. Takahashi, *J. Mater. Sci.* **22,** 2993 (1987).
13. J. L. Pouchou and F. Pichoir, *J. Microsc. Spectrosc. Electron.* **10,** 279 (1985).
14. Nonius Kappa CCD Program Package COLLECT, DENZO, SCALEPACK, SORTAV, Nonius Delft, The Netherlands, 1998.
15. G. M. Sheldrick, SHELX-97, Program for Crystal Structure Refinement, University of Göttingen, Germany (1997); Windows version by McArdle, Natl. Univ. Ireland, Galway.
16. J. Rodriguez-Carvajal, "FULLPROF: A Program for Rietveld Refinement and Pattern Matching Analysis," Abstracts of the Satellite Meeting on Powder Diffraction of the XV Congr. Intl. Union of Crystallogr., Talence, France, p. 127, 1990.
17. G. Venturini, I. Ijjaali, and B. Malaman, *J. Alloys Compds.* **284,** 262 (1999).
18. G. Venturini, I. Ijjaali, and B. Malaman, *J. Alloy Compds.* **289,** 116 (1999).
19. B. C. Sales and D. K. Wohlleben, *Phys. Rev. Lett.* **35,** 1240 (1975).
20. J. M. Lawrence, P. S. Riseborough, and R. D. Parks, *Rep. Prog. Phys.* **44,** 1 (1981).
21. K. Kadowaki and S. B. Woods, *Solid State Commun.* **58,** 507 (1986).
22. D. K. Wohlleben and B. Wittershagen, *Adv. Phys.* **34,** 403 (1985).
23. E. Parthé, L. Gelato, B. Chabot, M. Penzo, K.Cenzual, and R. Gladyshevskii, "Typix-Standardized Data and Crystal Chemical Characterization of Inorganic Structure Types," Vol. 1, p. 233, Table E52; part of the "Gmelin Handbook of Inorganic and Organometallic Chemistry," 8th ed. Springer-Verlag, Berlin, 1994.
24. P. Villars and L. D. Calvert, "Pearsons Handbook of Crystallographic Data for Intermetallic Phases," 2nd Ed. ASM International, Materials Park, OH, 1991.